Phenylpropionc acid produced by gut microbiota alleviates acetaminophen-induced hepatotoxicity

Sungjoon Cho[1], Kyoung-Jae Won[2], Xiaotong Yang[1], Vanessa Leone[3], Nathaniel Hubert[2], Eugene Chang[3], Eunah Chung[4], Joo-Seop Park[4], Hyunwoo Lee[1, a], Hyunyoung Jeong[1, a]

[1] Department of Pharmaceutical Sciences, College of Pharmacy, University of Illinois at Chicago, Chicago, IL, 60607, USA

[2] Departments of Pharmacy Practice, College of Pharmacy, University of Illinois at Chicago, Chicago, IL, USA

[3] Section of Gastroenterology, Knapp Center for Biomedical Discovery, University of Chicago, Chicago, IL, USA

[4] Division of Pediatric Urology and Division of Developmental Biology, Cincinnati Children's Hospital Medical Center, Cincinnati, OH 45229, University of Cincinnati College of Medicine, Cincinnati, OH 45267, USA

[a] Corresponding author

Correspondence: Hyunyoung Jeong, PharmD, PhD

Hyunwoo Lee, PhD

Department of Pharmaceutical Sciences

University of Illinois at Chicago

900 South Ashland Ave, Chicago, IL 60607

Phone: 312-996-7820, 312-996-3371

E-mail: yjeong@uic.edu, hlee31@uic.edu

ABSTRACT

Acetaminophen (APAP) overdose causes hepatic injury. To investigate potential roles of gut microbiota in APAP-induced liver injury, C57BL/6 mice from Jackson (JAX) or Taconic (TAC) were challenged with APAP. TAC mice were more susceptible to APAP toxicity, and this disappeared upon co-housing of JAX and TAC mice. When the cecum contents from JAX and TAC mice were transplanted into germ-free mice, the mice that received JAX gut microbiota exhibited less toxicity after APAP administration. Unbiased metabolomic analysis using portal vein serum and liver tissue of the mice led to identification of 19 metabolites whose levels differ between JAX and TAC mice as well as between mice transplanted with JAX or TAC gut microbiota, and this includes gut bacteria-derived metabolite phenylpropionic acid (PPA). PPA levels in cecum and portal vein were higher in mice harboring JAX gut microbiota. PPA supplementation in drinking water led to decreased APAP toxicity in TAC mice. This illustrates a gut microbe-liver interaction mediated by a gut bacteria-derived metabolite in modulating drug-induced liver injury.

INTRODUCTION

Human gut carries ~100 trillions of bacteria that belong to >100 different species (1). Human gut microbes outnumber human cells by 3 times, and their gene pool size is 100-fold bigger than human genome (1). These gene products are involved in generation of thousands of chemically diverse small molecules from food (2, 3), many of which are bioactive and mediate the intricate interactions between gut microbes and host. For example, short chain fatty acids (SCFA; up to ~100 mM in the gut (4)) modulate host immune and metabolic systems through G protein-coupled receptors (GPR) 41 and 43 (5) while aromatic acid amino acid metabolites, such as indole propionic acid, regulate intestinal permeability and systemic immunity (6, 7).

Diet as well as metabolic gene contents among gut microbial communities can govern the levels of gut microbial metabolites (3, 6, 8, 9). Recent studies have demonstrated that the metabolic output of gut microbiota, given the same diet, can be controlled by different strategies. These include chemical inhibition of microbial enzymes mediating the metabolite production (10, 11) or introduction of engineered bacteria strains into the complex microbial communities (6, 12). Engineered regulatory systems to control gene expression in human gut commensal bacteria have also been introduced (13). Together, gut microbiota is an emerging and promising target that can be engineered to improve human health. What remains lacking is detailed understanding about the biological functions and the underlying molecular mechanisms for most gut bacteria-derived metabolites (3, 14).

APAP is a commonly used analgesic but can cause fulminant acute liver failure upon overdose. APAP is the major cause of acute liver failure in the US (15, 16). APAP is mainly eliminated as inactive sulfate or glucuronide conjugates into the urine. APAP toxicity is triggered by its bioactivation by cytochrome P450 (CYP) 2E1 (major), CYP3A4, and CYP1A2 to a toxic metabolite *N*-acetyl-*p*-benzoquinone imine (NAPQI). NAPQI is a strong oxidizing agent and interacts with glutathione, leading to glutathione depletion in the liver. This subsequently leads to NAPQI binding to cellular components (e.g., proteins), oxidative stress, activation of JNK (c-Jun-N-terminal kinase) signaling, and cell necrosis.

Acute liver injury after APAP ingestion exhibits large interindividual variability (17). This is not fully explained by currently available knowledge such as genetic polymorphisms in phase I and phase II enzymes (15, 18-23). Results from previous studies suggest that altered gut microbiota may impact the susceptibility to APAP hepatotoxicity. Metabolomics results of pre- and post-dose urinary metabolite profiles after the administration of a therapeutic dose of APAP suggest that gut bacteria metabolite *p*-cresol may competitively inhibit APAP sulfonation and potentially diverting APAP towards CYP-mediated bioactivation (24). Diurnal variations in gut microbiota abundance and composition were shown to be associated with altered susceptibility to APAP-induced hepatotoxicity (25, 26). Also, a probiotic *Enterococcus lactis* IITRHR1 was shown to alleviate APAP hepatotoxicity potentially by its antioxidant effects (27). Despite the accumulating evidence, systematic investigation of the roles of gut microbiota in APAP-induced hepatotoxicity and detailed mechanistic investigations have been lacking.

In this study, we demonstrated that differential gut microbiota alters susceptibility to APAP-induced hepatotoxicity in mice. Using unbiased metabolomics profiling, we identified a gut microbe-associated metabolite that alleviates APAP hepatotoxicity.

MATERIALS AND METHODS

Animals. Male or female C57BL/6 mice were purchased from Jackson laboratory (hereafter JAX; Sacramento, CA) or Taconic biosciences (hereafter TAC; Cambridge city, IN) and maintained in specified pathogen free state and fed a standard chow diet (Teklad 7012, Envigo). After one week of acclimation, mice were overnight fasted (14 h) and treated with APAP (300 mg/kg, intraperitoneal injection) or PBS. Food was returned to the mice after treatment. Mice were sacrificed 24 h after treatment. For cohousing, male C57BL/6 mice (4 weeks of age) from JAX or TAC were cohoused with mice from either the same or different vendors (4 mice/cage). After 4 weeks of cohousing, mice were overnight fasted and sacrificed. For supplementation of drinking water with 3-phenylpropionic acid (PPA), PPA were dissolved in drinking water at the final concentration of 0.4% (w/v), followed by pH adjustment. C57BL/6 mice from TAC (6-7 weeks of age) had free access to drinking water. After 4 weeks, mice were overnight fasted and sacrificed. All procedures were approved by the Institutional Animal Care and Use Committee in the University of Illinois at Chicago.

For gut microbiota transplantation, C57BL/6 germ-free (GF) mice (8-12 weeks of age) from University of Chicago were used. Cecum materials were collected from JAX or TAC mice (8-9 weeks of age; housed at University of Illinois at Chicago) and suspended in PBS (100 mg/mL). After homogenization, solutions were centrifuged to remove debris, and 200 μL of supernatant were orally administered into GF mice. Mice were fed a standard chow diet (Lab diet® 6F 5K67, Lab diet). After 4 weeks, mice were overnight fasted and sacrificed. All experimental animal procedures using GF mice were approved by the University of Chicago Animal Care and Use Committee.

Liver histology and measurement of ALT. Liver tissues were fixed with 10% neutral buffered formalin. Fixed liver tissues were embedded in paraffin. Sections were cut and stained with hematoxylin and eosin (H/E). Serum ALT levels were measured using ALT kit (A7526-150, Pointe Scientific, MI) according to the manufacturer's instruction.

Fecal bacteria genomic DNA extraction. Fecal pellets were collected before fasting, snap-frozen, and stored at -80°C until analysis. Genomic DNA was extracted from the samples using a Tissue DNA Purification Kit, implemented on a Maxwell® 16 automated extraction system (Promega). Genomic DNA quantity was assessed using a Qubit 2.0 fluorometer with the dsDNA BR Assay (Life Technologies, Grand Island, NY).

High-throughput 16S rRNA gene amplicon sequence libraries and data analysis. The V4 region of the 16S rRNA gene was amplified and sequenced at the High-Throughput Genome Analysis Core at Argonne National Laboratory. Briefly, PCR amplicon libraries targeting the 16S rRNA encoding gene present in metagenomic DNA are produced using a barcoded primer set adapted for the Illumina HiSeq2000 and MiSeq (28). DNA sequence data is then generated using Illumina paired-end sequencing at the Environmental Sample Preparation and Sequencing Facility (ESPSF) at Argonne National Laboratory. Specifically, the V4 region of the 16S rRNA gene (515F-806R) is PCR amplified with region-specific primers that include sequencer adapter sequences used in the Illumina flowcell (28, 29). The forward amplification primer also contains a twelve-base barcode sequence that supports pooling of up to 2,167 different samples in each lane (28, 29). Each 25 µL PCR reaction contains 9.5 µL of MO BIO PCR Water (Certified DNA-Free), 12.5 µL of QuantaBio's AccuStart II PCR ToughMix (2x concentration, 1x final), 1 µL Golay barcode tagged Forward Primer (5 µM concentration, 200 pM final), 1 µL Reverse Primer (5 µM concentration, 200 pM final), and 1 µL of template DNA. The conditions for PCR are as follows: 94 °C for 3 minutes to denature the DNA, with 35 cycles at 94 °C for 45 s, 50 °C for 60 s, and 72 °C for 90 s; with a final extension of 10 min at 72 °C to ensure complete amplification. Amplicons are then quantified using PicoGreen (Invitrogen) and a plate reader (Infinite® 200 PRO, Tecan). Once quantified, volumes of each of the products are pooled into a single tube so that each amplicon is represented in equimolar amounts. This pool is then cleaned up using AMPure XP Beads (Beckman Coulter), and then quantified using a fluorometer (Qubit, Invitrogen). After quantification, the molarity of the pool is determined and diluted down to 2 nM, denatured, and then diluted to a final concentration of 6.75 pM with a 10% PhiX spike for

sequencing on the Illumina MiSeq. Amplicons are sequenced on a 151bp x 12bp x 151bp MiSeq run using customized sequencing primers and procedures (28).

Quantitative Insights into Microbial Ecology 2 (QIIME2) software (https://qiime2.org/) was used to analyze the sequencing data. Forward, reverse and barcodes sequences were imported into an artifact type of EMPPairedEndSequences and demultiplexed (30). Demultiplexed reads were denoised with DADA2 (31) generating operational taxonomic units (OUT) table. Taxonomic annotations for each OTU were generated with the taxonomy classifier trained on the Greengenes18_3 97% OTUs where the sequences have been trimmed to include bases from the region of the 16S that was sequenced in this analysis (the V4 region, bound by the 515F/806R primer pair) (32). Taxonomic and OTU abundance data were generated for all phyla, classes, orders, families, genera, and species. Nonmetric multidimensional scaling (NMDS) plot, analysis of similarities (ANOSIM) and Shannon-index was created or calculated using the R package 'ggplot' and 'vegan'.

Measurement of APAP-sulfate and *p*-cresol sulfate level in the liver. Liver tissues (~50 mg) were homogenized in 450 μL of ice-cold MeOH followed by centrifugation at 16,000*g* for 10 min under 4°C. Supernatants were filtered through 0.22 μm pore Ultrafree-MC filter and stored at -80 °C until further use. Filtrates (50 μL) were mixed with 200 μL of MeOH containing internal standards (mixtures of APAP-d4 and APAP-sulfate-d3 and *p*-cresol-sulfate-d7) and centrifuged at 16,000*g* for 10 min under 4°C, and supernatants were used for LC-MS/MS analysis.

The levels of APAP-sulfate in the liver filtrate were measured using LC-MS/MS in positive ion mode and p-cresol sulfate were measured in negative ion mode. The separation was performed on a Atlantis T3 column (3 μm, 100 mm x 3 mm, i.d., Waters Corp., Milford, MA). Chromatographic separation was performed using 0.1 % formic acid in water (solvent A) and 0.1 % formic acid in acetonitrile (solvent B) at a flow rate of 0.4 mL/min. The gradient elution profile used is as follows: 95% A for 3 min, 95% to 10% A over 3 min, 10% A for 3 min, 10% to 95% A over 0.5 min, and 95% A for 5 min. The detection and quantification of analytes were accomplished by multiple reactions monitoring of 232.1/152.1 for APAP-

sulfate, 235.1/155.1 for APAP-sulfate-d3, 328.1/152.1, 187/107 for *p*-cresol sulfate, and 194/114 for *p*-cresol sulfate-d7.

High throughput RNA sequencing. Total RNA was isolated from liver tissues (n=4-5 mice/group) using Trizol (ThermoFisher Scientific). Concentration was measured by nanodrop (ThermoFisher Scientific) at 260 nm. RNA samples (n=3/group) from 4 groups of mice were used for RNA sequencing. From 5 μg of total RNA, mRNA was isolated using NEBNext Poly(A) mRNA Magnetic Isolation Module (cat. No. E7490, New England Biolabs, Ipswich, MA) following manufacturer's instructions. Fragmentation of RNA followed by reverse transcription and second strand cDNA synthesis was performed using NEBNext Ultra RNA Library Prep Kit for Illumina (cat. No. E7530, NEB). The resulting double-stranded cDNA's were further processed to DNA sequencing libraries using ThruPLEX DNA-seq 12S Kit (Rubicon Genomics, Ann Arbor, MI). Libraries were selected by gel purification for an average size of 350 bp. Each purified library was quantified using a Qubit fluorometer (Life Technologies) and equal amounts of each library were pooled and sequenced on the Illumina HiSeq 2500. All RNA sequencing reads were aligned to mm9 using Tophat. The mRNA abundance was expressed as Counts Per Million (cpm).

Measurement of short chain fatty acids (SCFAs) in mouse cecum. Mouse cecum content (~50 mg) was mixed with 250 μL of 50% aqueous acetonitrile, vortexed for 10 s and centrifuged at 16,000*g* for 15 min at 4 °C. Supernatant (200 μL) was collected and analyzed. Briefly, mixed standard solutions containing equal amount of individual SCFA at desired concentration were made in 50% acetonitrile. For derivatization, 40 μL of each standard solution or of each the supernatant were mixed with 20 μL of 10 mM 3-NPH in 50% ACN and 20 μL of 120 mM EDC in the same solution, incubated for 30min at 40°C, and 10% ACN (1 mL) was added. Diluted reaction solution was mixed with pre-made stable isotope labeled standards for LC/MS. The LC/MS analysis was performed on AB Sciex Qtrap 5500 coupled to Agilent UPLC/HPLC system. All samples are analyzed by Agilent poroshell 120 EC-C18 Column, 100Å, 2.7 μm, 2.1 mm X 100 mm coupled to an Agilent UPLC/HPLC system, which was operated at a flow rate of 400 μL/min. A gradient of solvent A (water, 0.1% formic acid) and solvent B (acetonitrile, 0.1% formic acid) was applied

as: 0 min, 30% of solvent B; increase solvent B to 100% over 4 min; maintain solvent B at 100% for 5 min. The column was equilibrated for 3 min at 30% solvent B between the injections. The column temperature was 25°C and the autosampler was kept at 4 °C. The detection and quantification of analytes were accomplished by multiple reactions monitoring of *m/z* 136.1/94.1 for acetate, 142.1/100.1 for heavy acetate, 150.1/94.1 for propionate, 156.1/100.1 for heavy propionate, 164.1/94.1 for butyrate and 170.1/100.1 for heavy butyrate. All the samples were analyzed by triplicate.

Measurement of 3-phenylpropionic acid in mouse cecum and serum. Mouse cecum content (~50 mg) was mixed with 250 µL of 50% aqueous acetonitrile, vortexed for 10 s and centrifuged at 16,000*g* for 15 min at 4 °C. Supernatants were collected, diluted with 50% acetonitrile by 20 fold, and mixed with ice-cold acetonitrile containing *t*-cinnamic acid-d6 (100 ng/mL) as an internal standard followed by centrifugation at 16,000*g* for 10 min at 4 °C. Supernatants were filtered through 0.22 µm pore Ultrafree-MC filter and used for LC-MS/MS analysis. PPA-d9 was used as a surrogate standard to construct the calibration curve for the quantification of PPA (33).

Mouse serum collected from portal vein or heart was diluted with double distilled water (DDW) by 3 fold and mixed with ice-cold ACN containing 100 ng/ml of *trans*-cinnamic acid-d6 followed by centrifugation at 16,000*g* for 10 min at 4°C. Supernatants were dried and reconstituted with 70:30 mixture of water (0.01% acetic acid) and acetonitrile (0.01% acetic acid).

The levels of PPA in the cecum filtrates or serum were measured using LC-MS/MS in negative ion mode. The separation was performed on Atlantis T3 column (3 µm, 100 mm x 3 mm, i.d., Waters Corp., Milford, MA). Chromatographic separation was performed using 0.01 % acetic acid in water (solvent A) and 0.01 % acetic acid in acetonitrile (solvent B) at a flow rate of 0.4 mL/min. The gradient elution profile used is as follows: 70% solvent A for 0.5 min, 70% to 10% solvent A over 5 min, 10% solvent A for 4 min, 10% to 70% solvent A over 0.1 min, and 70% solvent A for 5.4 min (15 min analysis in total). The detection and quantification of analytes were accomplished by multiple reactions monitoring of *m/z* 149.0/105.0 for PPA, 158.0/114.2 for PPA-d9, and 152.9/109.1 for CA-d6.

Non-targeted metabolomics. Portal vein serum and liver tissues were collected before APAP administration from conventional JAX and TAC mice as well as JAX_{GF} and TAC_{GF} mice (n=5 mice/group). Respective samples from GF mice (n=3/group) were also included as a control. Samples were immediately snap frozen in liquid nitrogen and stored at -80 °C. Samples were prepared using the automated MicroLab STAR® system from Hamilton Company and analyzed via UPLC-MS/MS by Metabolon, Inc. To remove protein, dissociate small molecules bound to protein or trapped in the precipitated protein matrix, and to recover chemically diverse metabolites, proteins were precipitated with methanol under vigorous shaking for 2 min (Glen Mills GenoGrinder 2000) followed by centrifugation. The resulting extract was divided into five fractions: two for analysis by two separate reverse phase (RP)/UPLC-MS/MS methods with positive ion mode electrospray ionization (ESI), one for analysis by RP/UPLC-MS/MS with negative ion mode ESI, one for analysis by HILIC/UPLC-MS/MS with negative ion mode ESI, and one sample was reserved for backup. Samples were placed briefly on a TurboVap® (Zymark) to remove the organic solvent. The sample extracts were stored overnight under nitrogen before preparation for analysis. For UPLC-MS/MS analysis, all methods utilized a Waters ACQUITY UPLC and a Thermo Scientific Q-Exactive high resolution/accurate mass spectrometer interfaced with a heated electrospray ionization (HESI-II) source and Orbitrap mass analyzer operated at 35,000 mass resolution. The sample extract was dried then reconstituted in in solvents compatible to each of the four methods. Each reconstitution solvent contained a series of standards at fixed concentrations to ensure injection and chromatographic consistency. One aliquot was analyzed using acidic positive ion conditions, chromatographically optimized for more hydrophilic compounds. In this method, the extract was gradient eluted from a C18 column (Waters UPLC BEH C18-2.1x100 mm, 1.7 µm) using water and methanol, containing 0.05% perfluoropentanoic acid (PFPA) and 0.1% formic acid. Another aliquot was also analyzed using acidic another positive ion conditions which was chromatographically optimized for more hydrophobic compounds. In this method, the extract was gradient eluted from the same afore mentioned C18 column using methanol, acetonitrile, water, 0.05% PFPA and 0.01% formic acid and was operated at an overall higher organic content. Another aliquot was analyzed using basic negative ion optimized conditions using a separate dedicated C18 column.

The basic extracts were gradient eluted from the column using methanol and water, however with 6.5 mM Ammonium Bicarbonate at pH 8. The fourth aliquot was analyzed via negative ionization following elution from a HILIC column (Waters UPLC BEH Amide 2.1x150 mm, 1.7 μm) using a gradient consisting of water and acetonitrile with 10 mM ammonium formate, pH 10.8. The MS analysis alternated between MS and data-dependent MS^n scans using dynamic exclusion. The scan range varied slighted between methods but covered 70-1000 *m/z*. Peaks were quantified using area-under-the curve. Detected metabolites were identified by comparison to library entries of purified standards. Following normalization to serum sample volume or liver tissue weight, log transformation and imputation of missing values, Welch's two-sample t-test was used to identify metabolites that significantly different between experimental groups.

Statistical analysis. Most data were expressed as mean ± standard deviation (SD). Comparisons between groups were made by using the Student's t-test or one-way ANOVA via GraphPad Prism 7. Spearman rank correlation test and false discovery rate (FDR) were calculated using R package 'multtest'. *P*-value or FDR value less than 0.05 was considered significant.

RESULTS

Differential gut microbiota modulates susceptibility to APAP toxicity. Mice raised in different environments are known to harbor distinct gut microbiota composition (34, 35). To determine whether differential gut microbiota modulates susceptibility to APAP toxicity, male C57BL/6 mice from two different vendors [Jackson (JAX) and Taconic (TAC)] were challenged with APAP. Considering the potential inter-facility variability in the susceptibility to APAP toxicity, APAP dose that exhibits prominent hepatotoxicity was first determined. Mice were treated with 100, 200 or 300 mg/kg APAP (or PBS) via intraperitoneal injection and sacrificed 24 h after treatment. Serum levels of ALT were measured as a marker of liver damage. All mice in the PBS or 100 mg/kg groups and about half of the mice in the 200 mg/kg group did not exhibit hepatotoxicity (Fig S1A). Accordingly, the APAP dose of 300 mg/kg was chosen for the study. At this dose, the extent of hepatotoxicity (i.e., serum ALT level) was much greater in TAC than JAX mice (Fig S1B). While a similar trend was also observed in female TAC and JAX mice, the severity of hepatotoxicity at the dose was less in female mice (Fig S1B), consistent with the previous reports (36). Throughout the study, male mice were used.

To explore the potential roles of gut microbiota in altered susceptibility to APAP hepatotoxicity, JAX and TAC mice were cohoused for 4 weeks (a process known to assimilate gut microbiota of mice) and challenged with APAP. This created two additional groups of mice, namely coJAX (i.e., JAX mice cohoused with TAC) and coTAC (i.e., TAC mice cohoused with JAX). At the end of 4-week cohousing, fecal samples were collected from each mouse, and gut microbiome was analyzed by 16S rRNA gene amplicon sequencing. Nonmetric multidimensional scaling (NMDS) plot showed that JAX mouse group was separated from TAC mice (p=0.002, ANOSIM) and while coJAX and coTAC groups clustered together (p = 0.276, ANOSIM) (Fig 1A), suggesting that JAX and TAC mice indeed had distinct gut microbiota composition and co-housing abrogated the difference. Similarly, the difference in Shannon-index (an indicator of species richness or α-diversity) between JAX and TAC mice disappeared upon cohousing (Fig S1C). Importantly, the difference in the serum ALT levels between JAX and TAC mice disappeared upon

co-housing (Fig 1B). The effects of co-housing on the differences in APAP-induced hepatotoxicity between JAX and TAC mice were further verified by histological analysis of liver tissues (Fig S1E).

Genetic drifts between C57BL/6 mice from JAX and TAC have been reported (37), potentially contributing to altered susceptibility in APAP-induced hepatotoxicity between JAX and TAC mice. To examine the roles of differential gut microbiota in APAP toxicity in the mice of the same genetic background, the gut microbiota from JAX or TAC mice was transplanted to GF mice, followed by APAP challenge. To this end, pooled cecum materials from JAX or TAC mice were orally administered into GF mice, followed by 4-week conventionalization period (hereafter called JAX_{GF} and TAC_{GF}, respectively). Fecal microbiome analysis after 4 weeks post-transplantation revealed that gut microbiota of JAX_{GF} and TAC_{GF} mice were distinct (p=0.001, ANOSIM) and co-clustered with their respective donor groups (Fig 1C). Also, Shannon-index of JAX_{GF} and TAC_{GF} were similar to that of donor mice, indicating that cecum material transplantation successfully established the donor's microbiome in GF mice (Fig S1D). When challenged with APAP, TAC_{GF} mice showed higher APAP toxicity compared to JAX_{GF}, recapitulating the phenotype observed in conventional JAX and TAC mice (Fig 1D). Similar results were obtained in the histological analysis of the liver tissues (Fig S1F). These results indicate that susceptibility to APAP-induced hepatotoxicity is transferable by gut microbiota.

Abundances of certain gut microbial taxa are associated with APAP toxicity. To understand how differential gut microbiota alters APAP-induced liver injury, the microbiota compositions in conventional and gut microbiota-transplanted mice were analyzed. At the phylum level, *Bacteroidetes* and *Firmicutes* accounted for the majority of bacteria (80-90%), consistent with a previous report (38). JAX gut microbiota was associated with significantly higher abundances of *Verrucomicrobia* while TAC microbiota with higher *Firmicutes* and *Deferribacteres* (Fig S2). At the family level, JAX gut microbiota was associated with higher abundances of *Porphyromonadaceae* and *S24-7* while TAC microbiota with higher abundances of *Deferribacteraceae*, *Clostridiaceae, Dehalobacteriaceae* and *Lactobacillaceae* (Fig S2), in part consistent with a previous report (39). At the genus level, TAC microbiota was more abundant in *Parabacteroides* and *Mucispirillum*, and less abundant in *Akkermansia*.

To identify bacteria taxa that are associated with the severity of APAP toxicity, correlations between relative abundance of bacteria at the genus level (based on 16S rRNA sequencing data from feces collected before APAP dosing) and serum ALT level (at 24 h post-dosing) were examined. The analysis was performed separately for two gut microbiome results obtained from the cohousing and the gut microbiota transplantation experiments. Gut microbiome from co-housing experiment revealed that fecal abundances of *Parabacteroides* and unclassified *Firmicutes* were positively associated with serum ALT level (Fig 2A). *Parabacteroides* was resolved to the species level (*Parabacteroides goldsteinii*; 8.351% vs. 0.001% in TAC and JAX, respectively). *Lactobacillus* abundance was positively associated with serum ALT levels although it did not reach statistical significance (i.e., FDR=0.07). The abundance of unclassified *S24-7* was negatively associated with APAP toxicity. The abundances of *Mucispirillum* and *Akkermansia* genera, the groups that differ between JAX and TAC mice, were found not associated with serum ALT levels when the abundance data from coJAX and coTAC were included to examine correlation. The associations between serum ALT levels and fecal abundance of these bacteria taxa did not reach statistical significance in the gut microbiota transplantation group (Fig 2B), potentially due to relatively small sample size.

Gut microbiota-derived metabolites reduce APAP toxicity. Gut microbiota produces thousands of chemically diverse small molecules, many of which are bioactive and influence host health and diseases (2, 3). Gut bacteria metabolite *p*-cresol may competitively inhibit APAP sulfonation, potentially diverting APAP towards CYP-mediated bioactivation (24). Basal hepatic *p*-cresol sulfate levels were higher in TAC than JAX mice (Fig S3A). On the other hand, hepatic APAP-sulfate levels (measured at 15 min after APAP dosing) were similar between TAC and JAX, and about 1000-fold higher than the *p*-cresol sulfate level (Fig S3B), suggesting that at a toxic dose of APAP, the competition of APAP sulfonation by *p*-cresol is unlikely.

Short chain fatty acids (SCFA) are major products of bacterial fermentation and modulate multiple aspects of host physiology (40-42). The cecum levels of major SCFAs, acetate and butyrate, were similar between JAX and TAC as well as JAX_{GF} and TAC_{GF} mice (Fig S2C). Propionate levels differ between JAX

and TAC, but this was not observed in gut microbiota-transplanted mice. These results suggest minor roles of these SCFAs, if any, in modulating APAP-induced hepatotoxicity.

For *de novo* identification of gut microbiota-associated metabolites associated with altered susceptibility to APAP hepatotoxicity, portal vein serum and liver tissues collected from JAX and TAC mice as well as JAX_{GF} and TAC_{GF} mice were subjected to unbiased metabolomic profiling using LC-MS/MS. Portal vein serum and liver tissue samples from GF mice were included as controls. A total of 789 and 669 compounds of known identity were detected in the liver and serum samples, respectively. A majority (i.e., 568 compounds) were detected in both liver and serum samples. Principal component analysis (PCA) of liver samples revealed good separation along component 1 between conventional (JAX and TAC) mouse and GF/microbiota-transplanted mouse groups (Fig 3A), likely reflecting the effects of different facilities (i.e., University of Illinois at Chicago and University of Chicago for conventional mice and gut microbiota-transplanted mice, respectively) on metabolomes. Additional segregation was observed for JAX and TAC samples, and for GF, JAX_{GF}, and TAC_{GF} groups. Hierarchical clustering analysis revealed separation of GF group (as expected), with further separation dictated by colonization status (i.e. conventionally raised vs. microbiota-transplanted mice). In agreement with the partial overlap observed in PCA, JAX_{GF} and TAC_{GF} samples were intermixed but showed group-related sub-clustering. Similar results were obtained from portal vein serum samples (Fig 3B). Taken together, these analyses indicate that in addition to GF status, the differences in microbiota structure can dictates host metabolomic profiles.

To compile a list of gut microbiota-associated metabolites that are potentially linked to altered APAP hepatotoxicity, the data were filtered through multiple layers of selection criteria. First, metabolites that showed statistically significant differences in their signals between JAX and TAC (either liver or serum) samples were selected. They were further filtered out by comparing their signals between JAX_{GF} and TAC_{GF} mice, using $p<0.05$ as a cut-off; only the metabolites that showed the same directional changes as in the conventional mice were selected. This led to a total of 26 and 17 compounds in the liver and portal vein serum samples, respectively. Ten and 9 compounds showed >2-fold differences in the liver and serum samples, respectively, leading to a total 19 compounds as potential candidates for modulating APAP-

induced hepatotoxicity (Fig 3C and 3D). Four compounds (i.e., stachydrine, betonicine, 3-ureidopropionate, and trigonelline) were detected in the serum samples of GF mice, suggesting that they may be produced mainly by the host. The rest were undetectable or detected at lower signals in GF serum (>3-fold as compared to conventional mice), suggesting that they may be produced by gut microbes. Consistent with results from the previous independent measurement (Fig S3A), the signals for *p*-cresol sulfate were higher in TAC than JAX mouse liver, supporting the robustness of the metabolome analysis.

Among 10 metabolites identified as being more abundant in the liver and portal vein serum of JAX mice, four were derived from the reductive metabolic pathway of phenylalanine (6): 3-phenylpropionic acid (PPA), phenylpropionyl glycine, cinnamoyl glycine, and hippuric acid (Fig 4A). Phenylalanine is metabolized by gut bacteria to *trans*-cinnamic acid (CA) and subsequently to PPA. Once absorbed, CA and PPA are conjugated with glycine by glycine *N*-acyltransferase (43). PPA can also be further metabolized by β-oxidation to benzoic acid, which is conjugated with glycine to form hippuric acid (43). To identify the sources for the greater abundance of these metabolites in JAX tissues, CA and PPA contents in the mouse cecum were measured. CA was undetectable in the cecum samples, likely reflecting rapid conversion of CA to PPA by gut microbiota (6) and consistent with a previous report (44). PPA levels, on the other hand, were readily detectable in the mouse cecum contents, and 3.3-fold higher in JAX than TAC (Fig 4B). The PPA levels in mouse cecum contents were comparable to those in feces from healthy individuals (i.e., 267 nmole/g) (45). PPA was undetectable in GF mouse cecum contents, consistent with the idea that PPA is a gut microbial product and not present in the diet. JAX_{GF} mouse cecum contained about 10-fold higher PPA than TAC_{GF}, suggesting that gut microbiota composition governs the PPA levels in mouse cecum contents. Similar results were obtained in serum prepared from cardiac blood (Fig 4B). PPA levels in portal vein serum were ~4-fold higher than the systemic concentration (Fig 4C), indicating rapid elimination of PPA by the liver likely via glycine conjugation. PPA levels between cecum and portal (or systemic) blood exhibited excellent correlations (Fig S4A), suggesting that cecum PPA levels govern the host exposure to PPA.

To determine whether higher PPA levels decrease the susceptibility to APAP-induced hepatotoxicity, TAC mice were supplemented with PPA (0.4% in drinking water) for 4 weeks, followed by APAP challenge. PPA dose was determined based on (1) the average volume of daily water consumption for a mouse and (2) the previously reported pharmacokinetic profiles of cinnamic acid (46) (as the pharmacokinetic profiles of PPA are currently not available) to raise PPA exposure by about 5-fold. PPA supplementation had no effects on the amount of water intake or body weight gain of the mice (Fig S4B). The PPA dose used in this study led to ~3-fold increases in cecum and serum PPA levels in TAC mice (Fig 4D), the level approximating those in JAX mice. When the mice were challenged with APAP, the PPA group exhibited significantly lower liver injury at 24 h post-dosing (Fig 4E), indicating that PPA supplementation alleviates APAP-induced hepatotoxicity.

DISCUSSION

Gut microbiota produces thousands of chemically diverse small molecules (2, 3), yet the biological functions and the underlying molecular mechanisms for most are largely unknown. Here we report that differential gut microbiota modulates susceptibility to APAP-induced hepatotoxicity in mice, and this is potentially mediated by a gut bacteria-derived metabolite PPA.

We found that C57BL/6 mice from TAC are more susceptible to APAP-induced hepatotoxicity than those from JAX. Similar results were previously reported (47, 48) although the underlying mechanisms remained unknown. Genetic drifts between C57BL/6 mice from JAX and TAC have been reported (37), including the deletion mutation in nicotinamide nucleotide transhydrogenase (*Nnt)* in JAX mice. *Nnt* encodes an enzyme involved in mitochondrial antioxidant defense (49), a biological function closely linked to APAP hepatotoxicity, raising the possibility that genetic variations between JAX and TAC may underlie the altered susceptibility to APAP toxicity. Of note, the differences in APAP toxicity was also accompanied by altered gut microbiota structure and composition. Cohousing of JAX and TAC abrogated the differences in the susceptibility to APAP toxicity. Furthermore, transplantation of JAX or TAC gut microbiota into GF mice recapitulated the differences in APAP toxicity between the conventional JAX and TAC mice,

indicating that susceptibility to APAP-induced hepatotoxicity is transferable by gut microbiota. While the potential involvement of genetic variations (between JAX and TAC) cannot be fully ruled out, the results from cohousing and gut microbiota transplantation experiments strongly support the idea that differential gut microbiota underlie the altered susceptibility to APAP-induced hepatotoxicity in mice. The bacteria abundances in *Parabacteroides* (specifically *Parabacteroides goldsteinii)* and *Lactobacillus* were found positively correlated with the APAP toxicity in this study.

Gut microbiota-derived metabolites are increasingly recognized as mediators of gut microbe-host interactions. *p*-Cresol is bacterial product of tyrosine that is readily conjugated by host sulfonation enzymes and excreted into the urine (50). After a therapeutic dose of APAP in humans, *p*-cresol sulfate in urine was found negatively correlated with urinary APAP-sulfate contents (24). Results from this study, however, indicate that the competition of sulfonation by *p*-cresol can be overcome when toxic doses of APAP are administered in mice, and thus the contribution of *p*-cresol to altered susceptibility to APAP hepatotoxicity appears minimal if any. Diurnal variations in gut microbiota abundance and composition were shown to be associated with altered susceptibility to APAP-induced hepatotoxicity, in part mediated by 1-phenyl-1,2-propanedione (PPD) (26). PPD is a gut bacteria product (26) and also a volatile flavoring ingredient present in plants (51). Likely due to further metabolism by gut microbes (26), the levels of this compound in the liver and cecum contents were reported to be very low (~50 pmol/g cecum or liver) and below the detection limits in our assays. Potential involvement of 1-phenyl-1,2-propanedione in altered susceptibility to APAP toxicity remains to be examined.

The unbiased metabolomic analyses of liver and portal serum samples collected from JAX and TAC as well as JAX_{GF} and TAC_{GF} mice suggest higher reductive metabolic activities of phenylalanine in JAX gut microbiota. PPA levels in the cecum *vs*. those in the portal vein and systemic circulation exhibited excellent positive correlation, suggesting that PPA production in the gut governs PPA exposure in the host. While the biological functions of PPA remain largely unknown, various structural analogues of PPA have been reported to have protective activities against chemical-induced liver injuries. 4-Phenylbutyric acid administered (30 min) after APAP dosing alleviated APAP-induced hepatotoxicity in mice, in part by

reducing endoplasmic reticulum stress (52). CA, the precursor of PPA, is shown to reverse ethanol-induced hepatotoxicity, apparently by lowering hepatic expression of inflammatory mediators and CYP2E1 (53). PPA may exert its protective activity observed in this study via as-yet-undefined mechanism(s) shared between PPA analogues.

A recent functional screening of gut bacterial metabolites for direct agonism of 241 G-protein coupled receptors has identified PPA as an agonist of GPR109B (aka HCA3) with the EC_{50} of 208 μM (45). Though this finding is interesting, GPR109B is a human-specific GPCR that is shown to sense other bacterial metabolites such as D-phenyllactic acid with the EC_{50} of 150 nM (54). GPRs are well known to have overlapping specificity for the same ligand (5), and the fact that GPR109B is absent in mice does not exclude the possibility that the protective activity of PPA against APAP hepatotoxicity may be, at least in part, mediated by a GPR. In this respect, it is notable that CA has been reported to be a ligand of GPR109A (aka HCA2) with the EC_{50} of 5-36 μM (55, 56). The potential involvement of GPR-mediated signaling in the mechanism of action of PPA remains to be determined.

PPA can be produced via different routes that involve the interaction between diet and gut bacteria as well as the interaction between gut bacteria. First, a reductive pathway in the gut bacterium *Clostridium sporogenes* is shown to metabolize phenylalanine into PPA (6, 57). The genes encoding enzymes mediating this reductive metabolism are also present in other gut bacteria such as *Peptostreptococcus anaerobius* (58). Therefore, the amount of PPA produced by gut bacterial metabolism of phenylalanine will be dependent on total numbers of gut bacteria harboring the reductive pathway genes and the availability of the substrate phenylalanine. Free phenylalanine in diet is absorbed mostly in the small intestine (59), and only a small fraction reaches the lower gastrointestinal tract. A large portion of phenylalanine available to gut bacteria in the large intestine is derived from proteolytic degradation of proteins by gut bacteria, which releases free phenylalanine or phenylalanine-containing peptides (60). Another source of phenylalanine in the large intestine is the biosynthesis of phenylalanine by gut bacteria (61). A recent study has shown that a major commensal gut bacteria, *Bacteroides thetaiotaomicron*, synthesizes *de novo* and excretes relatively large

amounts of phenylalanine into the gut lumen, and it exhibits high strain variation in production capacity (62). Therefore, the availability of phenylalanine to PPA-producing gut bacteria will depend not only on diet but also the composition of neighboring gut bacteria.

Second, it has been known that certain plant-derived chemicals, flavonoids, are degraded by gut bacteria into PPA. For example, isoflavones such as apigenin and naringenin are shown to be metabolized into 3-(4-hydroxyphenyl)propionic acid (4-HPPA) by the gut bacterium *Clostridium orbiscindens* (63), and dehydroxylation of 4-HPPA by other gut bacteria results in formation of PPA (64, 65). Apigenin, for example, exists as glycosides (e.g., apigenin-7-glucoside; A7G) in many vegetables, herbs, and beverages (66), and its availability to *C. orbiscindens* also requires prior removal of the sugar by gut bacterial glycosidases (67). Thus, the contribution of flavonoids such as apigenin to PPA production in the large intestine is governed by the interaction between the intake amounts of flavonoid glycosides, gut bacteria liberating the aglycone, and gut bacteria metabolizing the aglycone.

In conclusion, we have identified the gut bacterial metabolite PPA as one determinant of susceptibility to APAP-induced hepatotoxicity. Systemic levels of PPA appear to be well correlated with the amounts of PPA produced in the gut, perhaps suggesting the possibility of manipulating gut microbiota for PPA production.

CONFLICT OF INTEREST

The authors declare no conflict of interest.

ACKNOWLEDGMENTS

This work was funded by the Chicago Biomedical Consortium with support from the Searle Funds at The Chicago Community Trust.

REFERENCES

1. J. Qin *et al*., A human gut microbial gene catalogue established by metagenomic sequencing. *Nature* **464**, 59-65 (2010).
2. M. S. Donia, M. A. Fischbach, HUMAN MICROBIOTA. Small molecules from the human microbiota. *Science* **349**, 1254766 (2015).
3. A. Marcobal *et al*., A metabolomic view of how the human gut microbiota impacts the host metabolome using humanized and gnotobiotic mice. *The ISME journal* **7**, 1933-1943 (2013).
4. J. H. Cummings, E. W. Pomare, W. J. Branch, C. P. Naylor, G. T. Macfarlane, Short chain fatty acids in human large intestine, portal, hepatic and venous blood. *Gut* **28**, 1221-1227 (1987).
5. A. S. Husted, M. Trauelsen, O. Rudenko, S. A. Hjorth, T. W. Schwartz, GPCR-Mediated Signaling of Metabolites. *Cell Metab* **25**, 777-796 (2017).
6. D. Dodd *et al*., A gut bacterial pathway metabolizes aromatic amino acids into nine circulating metabolites. *Nature* **551**, 648-652 (2017).
7. M. Venkatesh *et al*., Symbiotic bacterial metabolites regulate gastrointestinal barrier function via the xenobiotic sensor PXR and Toll-like receptor 4. *Immunity* **41**, 296-310 (2014).
8. E. Holmes *et al*., Human metabolic phenotype diversity and its association with diet and blood pressure. *Nature* **453**, 396-400 (2008).
9. R. Liu *et al*., Gut microbiome and serum metabolome alterations in obesity and after weight-loss intervention. *Nat Med* **23**, 859-868 (2017).
10. A. B. Roberts *et al*., Development of a gut microbe-targeted nonlethal therapeutic to inhibit thrombosis potential. *Nat Med* **24**, 1407-1417 (2018).
11. B. D. Wallace *et al*., Alleviating cancer drug toxicity by inhibiting a bacterial enzyme. *Science* **330**, 831-835 (2010).
12. V. M. Isabella *et al*., Development of a synthetic live bacterial therapeutic for the human metabolic disease phenylketonuria. *Nat Biotechnol* **36**, 857-864 (2018).
13. B. Lim, M. Zimmermann, N. A. Barry, A. L. Goodman, Engineered Regulatory Systems Modulate Gene Expression of Human Commensals in the Gut. *Cell* **169**, 547-558.e515 (2017).
14. M. A. Fischbach, Microbiome: Focus on Causation and Mechanism. *Cell* **174**, 785-790 (2018).
15. A. M. Larson *et al*., Acetaminophen-induced acute liver failure: results of a United States multicenter, prospective study. *Hepatology* **42**, 1364-1372 (2005).
16. W. M. Lee, Acute liver failure in the United States. *Semin Liver Dis* **23**, 217-226 (2003).
17. N. Kaplowitz, Acetaminophen hepatoxicity: what do we know, what don't we know, and what do we do next? *Hepatology* **40**, 23-26 (2004).
18. L. L. Mazaleuskaya *et al*., PharmGKB summary: pathways of acetaminophen metabolism at the therapeutic versus toxic doses. *Pharmacogenet Genomics* **25**, 416-426 (2015).
19. L. E. Schmidt, K. Dalhoff, H. E. Poulsen, Acute versus chronic alcohol consumption in acetaminophen-induced hepatotoxicity. *Hepatology* **35**, 876-882 (2002).
20. D. C. Whitcomb, G. D. Block, Association of acetaminophen hepatotoxicity with fasting and ethanol use. *Jama* **272**, 1845-1850 (1994).
21. I. Kjartansdottir, O. M. Bergmann, R. S. Arnadottir, E. S. Bjornsson, Paracetamol intoxications: a retrospective population-based study in Iceland. *Scandinavian journal of gastroenterology* **47**, 1344-1352 (2012).
22. B. H. Rumack, R. C. Peterson, G. G. Koch, I. A. Amara, Acetaminophen overdose. 662 cases with evaluation of oral acetylcysteine treatment. *Archives of internal medicine* **141**, 380-385 (1981).

23. A. M. Moyer *et al*., Acetaminophen-NAPQI hepatotoxicity: a cell line model system genome-wide association study. *Toxicological sciences : an official journal of the Society of Toxicology* **120**, 33-41 (2011).
24. T. A. Clayton, D. Baker, J. C. Lindon, J. R. Everett, J. K. Nicholson, Pharmacometabonomic identification of a significant host-microbiome metabolic interaction affecting human drug metabolism. *Proceedings of the National Academy of Sciences of the United States of America* **106**, 14728-14733 (2009).
25. C. A. Thaiss *et al*., Microbiota Diurnal Rhythmicity Programs Host Transcriptome Oscillations. *Cell* **167**, 1495-1510.e1412 (2016).
26. S. Gong *et al*., Gut microbiota mediates diurnal variation of acetaminophen induced acute liver injury in mice. *Journal of hepatology* **69**, 51-59 (2018).
27. S. Sharma, J. Chaturvedi, B. P. Chaudhari, R. L. Singh, P. Kakkar, Probiotic Enterococcus lactis IITRHR1 protects against acetaminophen-induced hepatotoxicity. *Nutrition* **28**, 173-181 (2012).
28. J. G. Caporaso *et al*., Ultra-high-throughput microbial community analysis on the Illumina HiSeq and MiSeq platforms. *ISME J* **6**, 1621-1624 (2012).
29. J. G. Caporaso *et al*., Global patterns of 16S rRNA diversity at a depth of millions of sequences per sample. *Proceedings of the National Academy of Sciences of the United States of America* **108 Suppl 1**, 4516-4522 (2011).
30. E. Bolyen *et al*., QIIME 2: Reproducible, interactive, scalable, and extensible microbiome data science. *PeerJ Preprints* **6**, e27295v27291 (2018).
31. B. J. Callahan *et al*., DADA2: high-resolution sample inference from Illumina amplicon data. *Nature methods* **13**, 581 (2016).
32. N. A. Bokulich *et al*., Optimizing taxonomic classification of marker-gene amplicon sequences with QIIME 2's q2-feature-classifier plugin. *Microbiome* **6**, 90 (2018).
33. R. Thakare, Y. S. Chhonker, N. Gautam, J. A. Alamoudi, Y. Alnouti, Quantitative analysis of endogenous compounds. *J Pharm Biomed Anal* **128**, 426-437 (2016).
34. C. M. McIntosh, L. Chen, A. Shaiber, A. M. Eren, M.-L. Alegre, Gut microbes contribute to variation in solid organ transplant outcomes in mice. *Microbiome* **6** (2018).
35. A. Sivan *et al*., Commensal Bifidobacterium promotes antitumor immunity and facilitates anti-PD-L1 efficacy. *Science* 10.1126/science.aac4255 (2015).
36. K. Du, C. D. Williams, M. R. McGill, H. Jaeschke, Lower susceptibility of female mice to acetaminophen hepatotoxicity: Role of mitochondrial glutathione, oxidant stress and c-jun N-terminal kinase. *Toxicol Appl Pharmacol* **281**, 58-66 (2014).
37. A. J. Almodovar, R. J. Luther, C. L. Stonebrook, P. A. Wood, Genomic structure and genetic drift in C57BL/6 congenic metabolic mutant mice. *Mol Genet Metab* **110**, 396-400 (2013).
38. C. M. McIntosh, L. Chen, A. Shaiber, A. M. Eren, M. L. Alegre, Gut microbes contribute to variation in solid organ transplant outcomes in mice. *Microbiome* **6**, 96 (2018).
39. Ivanov, II *et al*., Induction of intestinal Th17 cells by segmented filamentous bacteria. *Cell* **139**, 485-498 (2009).
40. G. den Besten *et al*., The role of short-chain fatty acids in the interplay between diet, gut microbiota, and host energy metabolism. *J Lipid Res* **54**, 2325-2340 (2013).
41. R. L. Veech *et al*., The effect of short chain fatty acid administration on hepatic glucose, phosphate, magnesium and calcium metabolism. *Advances in experimental medicine and biology* **194**, 617-646 (1986).
42. H. Hara, S. Haga, Y. Aoyama, S. Kiriyama, Short-chain fatty acids suppress cholesterol synthesis in rat liver and intestine. *J Nutr* **129**, 942-948 (1999).
43. C. P. Badenhorst, E. Erasmus, R. van der Sluis, C. Nortje, A. A. van Dijk, A new perspective on the importance of glycine conjugation in the metabolism of aromatic acids. *Drug Metab Rev* **46**, 343-361 (2014).
44. I. Gutierrez-Diaz *et al*., Could Fecal Phenylacetic and Phenylpropionic Acids Be Used as Indicators of Health Status? *J Agric Food Chem* **66**, 10438-10446 (2018).

45. D. A. Colosimo *et al*., Mapping Interactions of Microbial Metabolites with Human G-Protein-Coupled Receptors. *Cell Host Microbe* **26**, 273-282 e277 (2019).
46. F. H.P., H. C.L., Z. L.T., L. R.F., Pharmacokinetics and Bioavailability of Cinnamic Acid in Mice. *J. China. Pharm. Univ.* **35**, 328-330 (2004).
47. M. Bourdi, J. S. Davies, L. R. Pohl, Mispairing C57BL/6 substrains of genetically engineered mice and wild-type controls can lead to confounding results as it did in studies of JNK2 in acetaminophen and concanavalin A liver injury. *Chemical research in toxicology* **24**, 794-796 (2011).
48. L. Duan *et al*., Differential susceptibility to acetaminophen-induced liver injury in sub-strains of C57BL/6 mice: 6N versus 6J. *Food Chem Toxicol* **98**, 107-118 (2016).
49. A. A. Toye *et al*., A genetic and physiological study of impaired glucose homeostasis control in C57BL/6J mice. *Diabetologia* **48**, 675-686 (2005).
50. E. A. Smith, G. T. Macfarlane, Enumeration of human colonic bacteria producing phenolic and indolic compounds: effects of pH, carbohydrate availability and retention time on dissimilatory aromatic amino acid metabolism. *J Appl Bacteriol* **81**, 288-302 (1996).
51. G. A. Burdock, *Encyclopedia of food and color additives* (CRC Press, Boca Raton, 1997).
52. H. Kusama *et al*., Sodium 4-phenylbutyric acid prevents murine acetaminophen hepatotoxicity by minimizing endoplasmic reticulum stress. *J Gastroenterol* **52**, 611-622 (2017).
53. S. L. Yan, Z. H. Wang, H. F. Yen, Y. J. Lee, M. C. Yin, Reversal of ethanol-induced hepatotoxicity by cinnamic and syringic acids in mice. *Food Chem Toxicol* **98**, 119-126 (2016).
54. A. Peters *et al*., Metabolites of lactic acid bacteria present in fermented foods are highly potent agonists of human hydroxycarboxylic acid receptor 3. *PLoS Genet* **15**, e1008145 (2019).
55. N. Ren *et al*., Phenolic acids suppress adipocyte lipolysis via activation of the nicotinic acid receptor GPR109A (HM74a/PUMA-G). *Journal of lipid research* **50**, 908-914 (2009).
56. J. P. van Veldhoven *et al*., Structure-activity relationships of trans-substituted-propenoic acid derivatives on the nicotinic acid receptor HCA2 (GPR109A). *Bioorg Med Chem Lett* **21**, 2736-2739 (2011).
57. S. R. Elsden, M. G. Hilton, J. M. Waller, The end products of the metabolism of aromatic amino acids by Clostridia. *Arch Microbiol* **107**, 283-288 (1976).
58. M. Wlodarska *et al*., Indoleacrylic Acid Produced by Commensal Peptostreptococcus Species Suppresses Inflammation. *Cell Host Microbe* **22**, 25-37 e26 (2017).
59. S. Broer, S. J. Fairweather, Amino Acid Transport Across the Mammalian Intestine. *Compr Physiol* **9**, 343-373 (2018).
60. K. Windey, V. De Preter, K. Verbeke, Relevance of protein fermentation to gut health. *Mol Nutr Food Res* **56**, 184-196 (2012).
61. J. Pittard, J. Yang, Biosynthesis of the Aromatic Amino Acids. *EcoSal Plus* **3** (2008).
62. H. Chen *et al*., A Forward Chemical Genetic Screen Reveals Gut Microbiota Metabolites That Modulate Host Physiology. *Cell* **177**, 1217-1231 e1218 (2019).
63. L. Schoefer, R. Mohan, A. Schwiertz, A. Braune, M. Blaut, Anaerobic degradation of flavonoids by Clostridium orbiscindens. *Appl Environ Microbiol* **69**, 5849-5854 (2003).
64. J. I. Mosele, A. Macia, M. J. Motilva, Metabolic and Microbial Modulation of the Large Intestine Ecosystem by Non-Absorbed Diet Phenolic Compounds: A Review. *Molecules* **20**, 17429-17468 (2015).
65. A. Braune, M. Blaut, Bacterial species involved in the conversion of dietary flavonoids in the human gut. *Gut Microbes* **7**, 216-234 (2016).
66. S. Bhagwat, D. B. Haytowitz, J. M. Holden (2014) USDA Database for the Flavonoid Content of Selected Foods. Release 3.1. in *USDA Database for the Flavonoid Content of Selected Foods* (U.S. Department of Agriculture, Agricultural Research Service).
67. L. Hanske, G. Loh, S. Sczesny, M. Blaut, A. Braune, The bioavailability of apigenin-7-glucoside is influenced by human intestinal microbiota in rats. *J Nutr* **139**, 1095-1102 (2009).

Figures

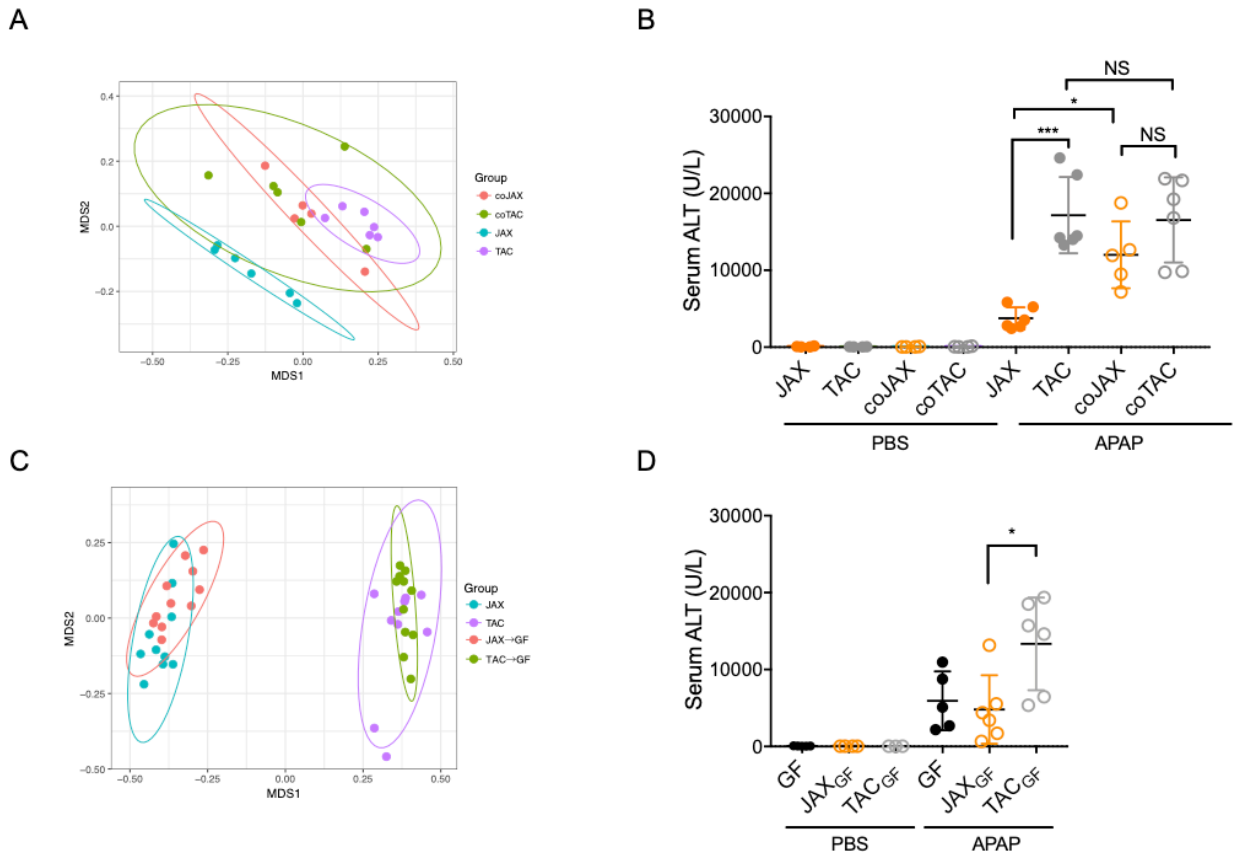

Fig 1. Differential gut microbiota modulates susceptibility to APAP-induced hepatotoxicity. A and B. C57BL/6 mice from JAX or TAC companies were co-housed with mice from the same or the other vendor for 4 weeks. (A) Gut microbiome was analyzed by 16S rRNA gene amplicon sequencing using fecal samples collected at the end of co-housing. Nonmetric multidimensional scaling (NMDS) plot is shown. (B) APAP (300 mg/kg or PBS, intraperitoneal injection) was administered after overnight fasting. Mice were sacrificed after 24 h, and serum ALT levels were measured as a measure of hepatotoxicity. **C and D**. Pooled cecum contents from JAX or TAC mice were orally administered into GF C57BL/6 mice. After 4 weeks, fecal samples were collected, and the mice were challenged with APAP (300 mg/kg or PBS, intraperitoneal injection). (C) NMDS plot based on 16S rRNA gene amplicon sequencing of the fecal samples is shown. APAP (300 mg/kg or PBS, intraperitoneal injection) was administered after overnight fasting. (D) Serum ALT levels at 24 h post-dosing are shown.

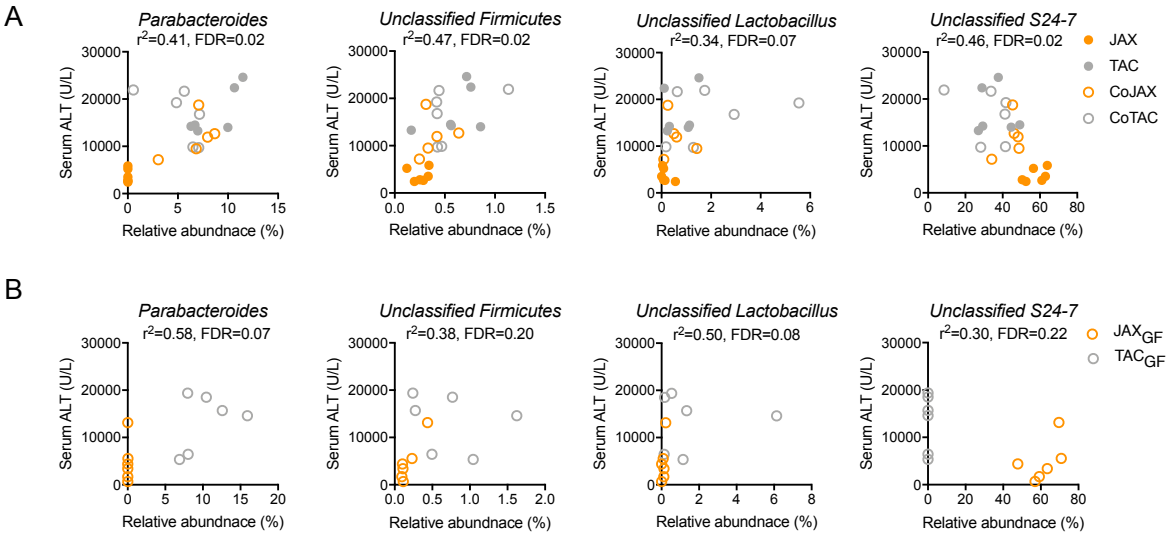

Fig 2. Fecal abundances of certain bacteria genus are associated with susceptibility to APAP-induced hepatotoxicity. A. C57BL/6 mice from JAX or TAC companies were co-housed with mice from the same or the other vendor for 4 weeks. Gut microbiome was analyzed by 16S rRNA gene amplicon sequencing using fecal samples collected at the end of co-housing. **B**. Pooled cecum contents from JAX or TAC mice were orally administered into GF C57BL/6 mice. After 4 weeks, fecal samples were collected and subjected to 16S rRNA gene amplicon sequencing.

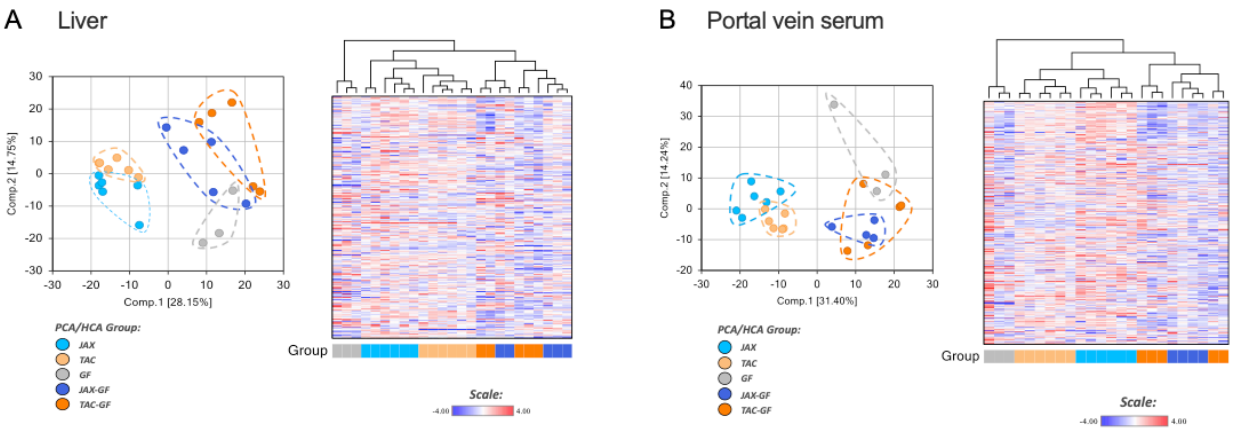

D

		Liver		Portal vein serum		
		TAC/JAX	TACGF/JAXGF	TAC/JAX	TACGF/JAXGF	CONV/GF
1	Cinnamoyl glycine	0.05	0.08	0.04	0.06	ND in GF
2	Phenylpropionyl glycine	0.13	0.12	0.05	0.05	ND in GF
3	2,8-Quinolinediol sulfate	0.15	0.14	ND	ND	ND in GF
4	3-Phenylpropionate	ND	ND	0.15	0.06	ND in GF
5	Hippurate	0.28	0.29	0.17	0.19	24
6	2-Amino-p-cresol sulfate	ND	ND	0.23	0.30	ND in GF
7	Stachydrine	0.34	0.48	0.60	0.79	1
8	Betonicine	0.43	0.43	1.14	0.84	1
9	3-Ureidopropionate	0.49	0.38	0.55	1.22	1
10	Trigonelline	0.49	0.39	0.59	0.77	1
11	N,N,N-Trimethyl-5-aminovalerate	1.7	2.4	2.2	4.1	8
12	Phenol sulfate	2.4	1.8	2.0	1.5	105
13	Phenol glucuronide	ND	ND	3.8	2.1	ND in GF
14	5-Aminovalerate	2.3	7.4	6.8	28.0	28
15	*p*-Cresol sulfate	4.4	12.6	4.7	10.6	12
16	3-(4-Hydroxyphenyl)propionate	ND	ND	6.0	30.6	ND in GF
17	2-Piperidinone	6.3	14.3	22.1	29.4	16
18	*p*-Cresol glucuronide	6.4	4.1	11.0	30.3	ND in GF
19	Dihydrocaffeate sulfate	36.7	98.3	82.4	255.4	ND in GF

Fig 3. Certain gut microbe-derived metabolites are associated with altered susceptibility to APAP-induced hepatotoxicity. Liver and portal vein serum samples from JAX, TAC, GF, JAX_{GF}, and TAC_{GF} were subjected to LC-MS/MS-based unbiased metabolomic profiling. **A and B**. Principal component analysis and hierarchical clustering analysis of liver (A) and portal vein serum (B) are shown. **C**. Schematics of filtering steps to compile a list of metabolites in liver and portal vein serum samples that are associated with altered APAP hepatotoxicity. **D.** The signal ratios for metabolites that exhibited significant differences between JAX and TAC as well as between JAX_{GF}, and TAC_{GF} mice are shown. CONV, conventional JAX or TC mice. ND, not detected.

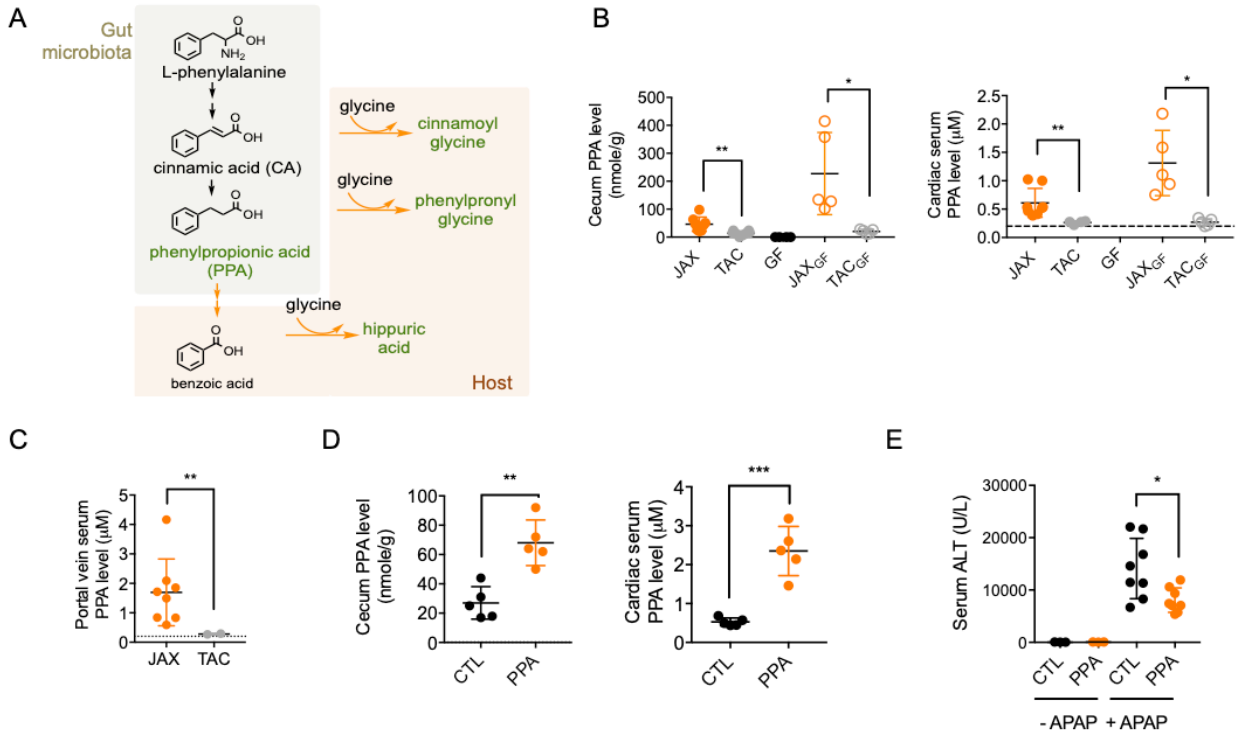

Fig 4. Gut microbe-associated metabolite, phenylpropionic acid (PPA), alleviates APAP hepatotoxicity. **A**. Gut microbe-mediated reductive metabolic pathway of phenylalanine and host-mediated glycine conjugation. Green color, the metabolites identified to be associated with altered APAP toxicity. **B** and **C**. PPA levels in cecum contents and cardiac (B) or portal vein (C) serum of untreated mice were measured by LC-MS/MS. Dotted line denotes the limit of quantification (i.e., 0.2 μM). **D.** C57BL/6 mice from TAC were given access to PPA (0.4% in drinking water) or control (CTL) water for 4 weeks. PPA concentrations in cecum contents or serum prepared from cardiac blood were measured using LC-MS/MS. **E**. After PPA supplementation for 4 weeks, the mice were challenged with APAP (300 mg/kg or PBS, intraperitoneal injection) after overnight fasting, and sacrificed at 24 h post-dosing.

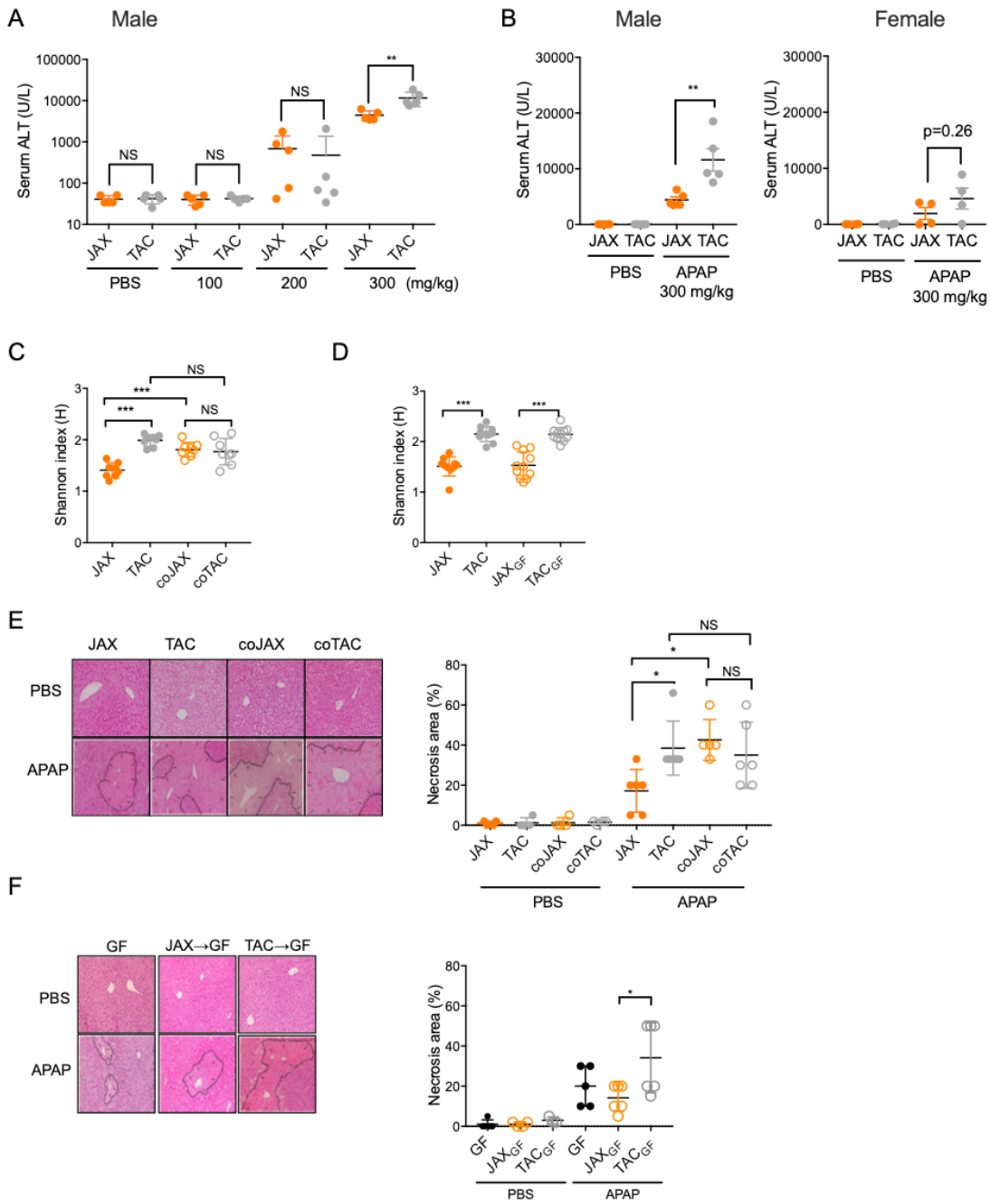

Fig S1. **A**. Male C57BL/6 mice from JAX or TAC received APAP (100, 200 or 300 mg/kg) or PBS intraperitoneally after overnight fasting. Mice were sacrificed after 24 h, and serum ALT levels were measured as a measure of hepatotoxicity. **B**. Male or female C57BL/6 mice received APAP (300 mg/kg or PBS, intraperitoneal injection) after overnight fasting, and serum ALT levels at 24 h post-dosing were measured. **C**. Gut microbiome was analyzed by 16S rRNA gene amplicon sequencing using fecal samples collected at the end of cohousing (4-week) or gut microbiota transplantation (oral gavage, followed by 4-week conventionalization). **E**. At the end of cohousing or gut microbiota transplantation, APAP (300 mg/kg or PBS, intraperitoneal injection) was administered after overnight fasting, and mice sacrified after 24 h. Liver tissue was H/E stained.

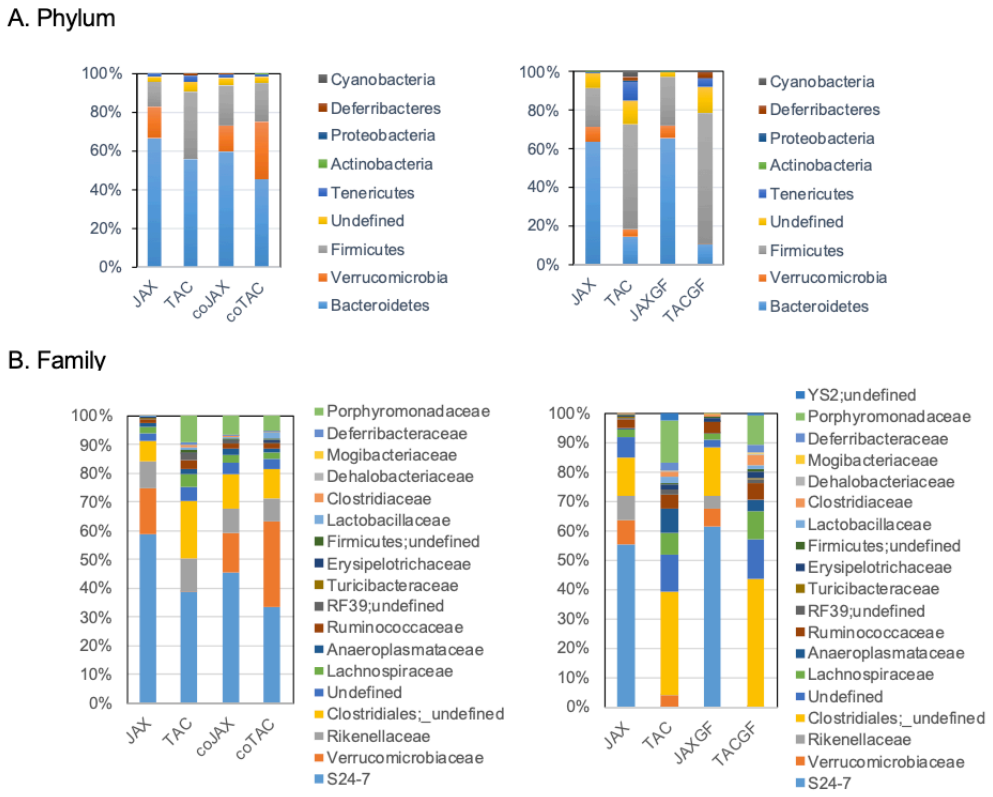

Fig S2. Gut microbiome of mice from co-housing (left) or gut microbiota-transplantation (right) experiments was analyzed by 16S rRNA gene amplicon sequencing. Gut bacteria compositions at phylum (A) and family (B) levels are shown.

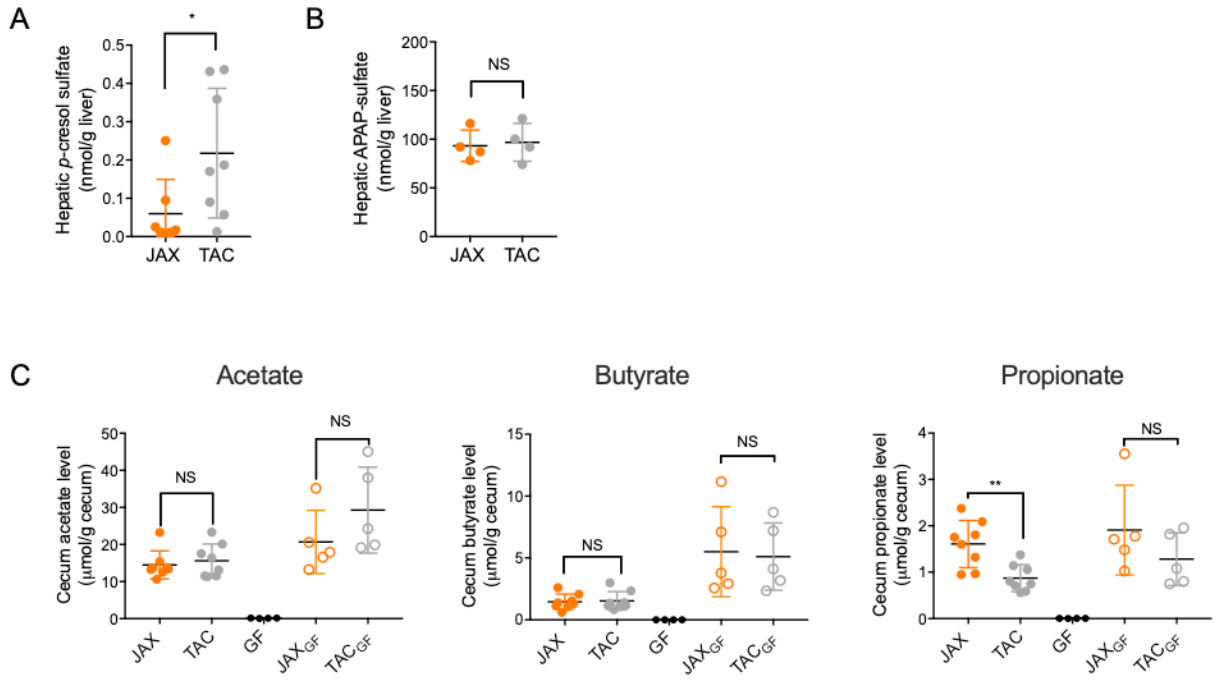

Fig S3. A. JAX or TAC mice were sacrificed after overnight fasting and liver tissues were collected. *p*-Cresol sulfate levels were measured using LC-MS/MS. **B.** C57BL/6 mice from JAX or TAC were administered with APAP (300 mg/kg, intraperitoneal injection), and the mice were sacrificed after 15 min. APAP-sulfate levels in the liver were measured using LC-MS/MS. **C.** Conventional JAX or TAC mice as well as gut microbiota-transplanted mice were sacrificed after overnight fasting and cecum contents were collected. The levels of major short chain fatty acids in the cecum contents were measured using LC-MS/MS.

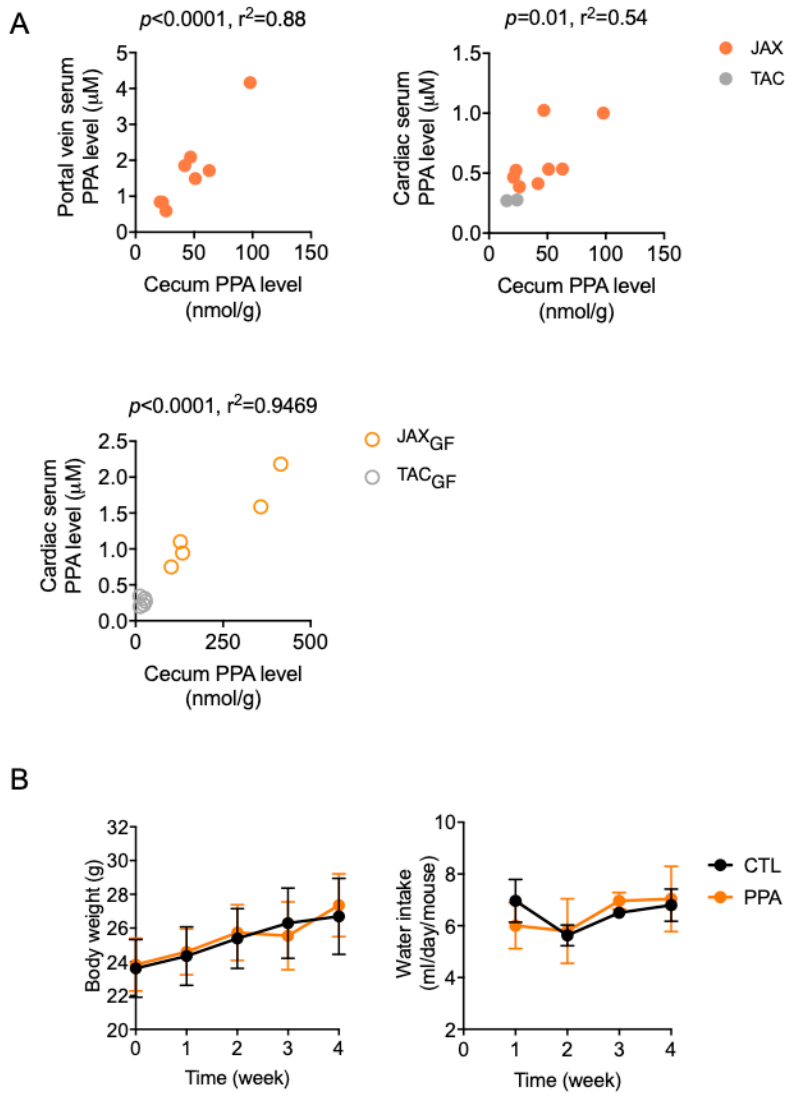

Fig S4. A. Correlations between PPA concentrations in cecum contents and serum prepared from portal vein (left) and cardiac blood (right) of JAX and TAC mice are shown. (bottom) Correlation between PPA concentrations in cecum contents and cardiac serum of JAX_{GF} and TAC_{GF} mice is shown. Mice that exhibited PPA concentrations below the quantification limit (i.e., 0.2 μM) are not included. **B**. TAC mice were fed with PPA (0.4% in drinking water) or regular water (CTL) for 4 weeks. Average body weight gain and water intake volume over time are shown.